Investigation of the drag reducing effect of hydrophobised sand on circular cylinders

J.C. Brennan[a1], D. J. Fairhurst[a], R. H. Morris[a], G. McHale[b] and M. I. Newton[a]

[a] School of Science and Technology, Nottingham Trent University, Clifton Lane, Nottingham, NG11 8NS, UK

[b] Faculty of Engineering & Environment, Northumbria University, Ellison Place, Newcastle upon Tyne, NE1 8ST, UK

Abstract

Superhydrophobic surfaces show strong potential for drag reducing applications. If such a surface supports a Cassie-Baxter state with low solid surface fraction and when immersed it retains a plastron air layer, large slip can occur across its surface and a consequent reduction in drag. In this work we report a facile method for creating hydrophobic cylinders and hydrophobic flat surfaces with varying surface roughness able to support a Cassie-Baxter state. Cylinders of 12mm diameter were coated in hydrophobised sand with grain sizes in the ranges 50-100µm, 212-300µm 425-600µm and 600-710µm to produce the different roughness. A Laser Doppler Anemometer was used to measure the velocity profile of the water across their wake in a large water circulating flow chamber. The hydrophobic cylinders in the Cassie-Baxter state show drag reductions of up to 28% compared to the same sample in the Wenzel state for

[1] Corresponding author: joseph.brennan@ntu.ac.uk

flows with Reynolds numbers of 10,000 to 40,000. These drag reduction results, in combination with confocal microscopy images of the plastron air layer and feature height, show that the thickness of the plastron and the protrusion height of the features combine to give a drag reduction or drag increase depending on the ratio of the two.

1. Introduction

Superhydrophobic surfaces are often found in nature and provide remarkable functionality, for example, self-cleaning Lotus leaves[1,2] and the underwater respiration of Fishing Spiders[3,4]. Recently there has been a large amount of research on using superhydrophobic surfaces on cylinders and on flat surfaces for drag reduction. This has been performed theoretically and with simulations[5-14] and experimentally[15-22]. All objects traveling through a fluid experience a drag force. Drag coefficient (C_D) is a dimensionless quantity that describes the drag on an object of a certain shape as it travels through a fluid. A low drag coefficient denotes a low drag force and a high drag coefficient denotes a high drag force. Two extreme superhydrophobic states can be achieved: one where the features on the surface do not penetrate into the liquid, the Cassie-Baxter state; and one where the features fully penetrate into the liquid, the Wenzel state. For a plastron air layer to be present the sample needs to be in the Cassie-Baxter state with the air layer retained between features forming the plastron. The drag reduction caused by a superhydrophobic surface is due to the presence of the plastron layer in the Cassie-Baxter state, which allows large water slip lengths across its surface[9,23,24]. In the Wenzel state the lack of this plastron layer leads to no drag reduction. The main limiting factor for superhydrophobic surfaces causing a drag reduction is the lifetime of the plastron layer[23]. This air layer may be removed from the surface through diffusion or stripped by the moving water passing over the surface.

There has been recent work into methods of retaining or replenishing the plastron air layer which would negate the effect of the lost plastron[26-28].

Work has previously been done on measuring the drag coefficients of smooth cylinders. In the Reynolds number range of 10,000 to 40,000, the drag coefficient of a plain rod is ~1 [29]. Drag coefficient results on cylinders with various roughness parameters, k/D = roughness scale/cylinder diameter, has also been widely researched[30-33]. When a roughened superhydrophobic surface has no plastron, the Wenzel state, it is effectively a rough surface. When the roughened superhydrophobic surface is in the Cassie-Baxter state, with the plastron air layer present, it cannot be viewed as a solid smooth rod or a roughened cylinder.

Confocal microscopy has been used to find the thickness of plastron layers[25,34] and the coverage of the plastron air layer[35]. By focusing on the substrate, the reflective air-water interface and the top of the features the height of features on the sample can be measured whilst at the same time measuring the thickness of the plastron that is retained between features.

In this report we outline a simple method for creating cylindrical rods and flat surfaces with hydrophobic surfaces possessing various levels of surface roughness. We use a large recirculating flow chamber with a Laser Doppler Anemometry (LDA) system to measure water velocities downstream of the sample being tested. Confocal microscopy was used to measure roughness feature height and plastron thickness. Results are presented that demonstrate a drag reduction when comparing a superhydrophobic

surface to a smooth plain surface and the same rough hydrophobic surface without the plastron air layer. We show that an increase in plastron thickness alone does not lead to a larger drag reduction, but that the ratio of the plastron thickness to the protrusion height of the roughness features above the plastron is the important factor.

2. Experimental details

Hydrophobic rods with various size features were constructed using brass rods with a diameter of 12mm and length of 21.5cm. These rods were made with a M6 bolt hole at one end and a M2 bolt hole at the other end, allowing the rod to be securely fastened into a large water circulating flow chamber with a base to top-of-pipe height of 3m and a total width of 2.3m. To create a hydrophobic coating for the rods, builder's sand was separated into various size fractions using sieves (Endecotts Ltd Laboratory test). The sieves had varying aperture sizes to form sand fractions of 50-100μm, 212-300μm, 425-600μm and 600-710μm. The sieved sand was also measured using a scanning electron microscope (Jeol Ltd, Tokyo, Japan) (SEM) to check the size distribution of sand grains. The sieved sand was cleaned using a solution of hydrochloric acid (Fisher Chemical 36%) and water in a ratio of 6:1 (v/v). Next, 20ml of sand was placed into a 50ml centrifuge tube and 25ml of the hydrochloric acid/water mix was added. The sand was left in the solution for 24 hours. The sand was then rinsed with water and dried in an oven at 80°C. The dried sand was hydrophobised using a solution of 5% commercial waterproofing product (Granger's Extreme Wash-In) and 95% warm water. The sand was left in the hydrophobising solution for 2 hours before the excess liquid was removed. The remaining wet sand was placed in an oven at 80°C for 8 hours to dry.

Polydimethylsiloxane (PDMS) (Dow Corning Sylgard 184) was mixed in a 10:1 (w/w) ratio of silicone elastomer to silicone curing agent. The PDMS was fully mixed and degassed before being poured onto the prepared rods. The rods were held vertically during the pouring of the PDMS. This allowed the PDMS to flow down the rod leading to complete coverage. The thickness of the PDMS on the rod was 100μm at the top of the rod and 110μm at the bottom. The rods were then placed in an oven at 60°C for 20 minutes at which point the PDMS became tacky but not fully cured. Whilst in this tacky state the sieved hydrophobised sand was tipped onto the rods as they were rotated so that it became partially embedded into the PDMS layer creating a homogenous layer of hydrophobised sand around the whole surface of the rod. The rods were then placed back into the oven at 60°C for another 4 hours to fully cure the PDMS. This was repeated for all 4 sand fractions. As well as hydrophobic sand rods, plain PDMS rods were made by pouring PDMS over the brass rod and fully curing the PDMS. Microscope slides were also made hydrophobic in the same way. These hydrophobised flat surfaces were then used to measure contact angles and for the plastron thickness experiments using the confocal microscope. The experimental setup for measuring the drag coefficient of a rod is illustrated schematically in Figure 1. A Laser Doppler Anemometer (LDA) was used to measure the velocity profile of the water downstream of the rods. The LDA used is a Dantec Dynamic Flow explorer mounted on a 3 axis traverse. The LDA traversed from 60mm from the centre of the rod on one side to 60mm from the centre of the rod on the other side travelling at right angles to the direction of the rod. Velocity measurements were taken at 3mm intervals across the 120mm distance. The same measurement profile was used to check the uniformity of the flow in the region where the sample was placed and at the point where the

measurements were taken. The results from this showed that in the area of interest the flow was laminar and uniform in velocity. The rods were tested in a plastron bearing state and after an ethanol pre-treatment which has the effect of wetting out the surface so that when it is place underwater there is no plastron air layer formed[15]. When the rods are ethanol pre-treated so that they do not have the plastron air layer they can be considered as a rough rod with water fully in contact with all features..

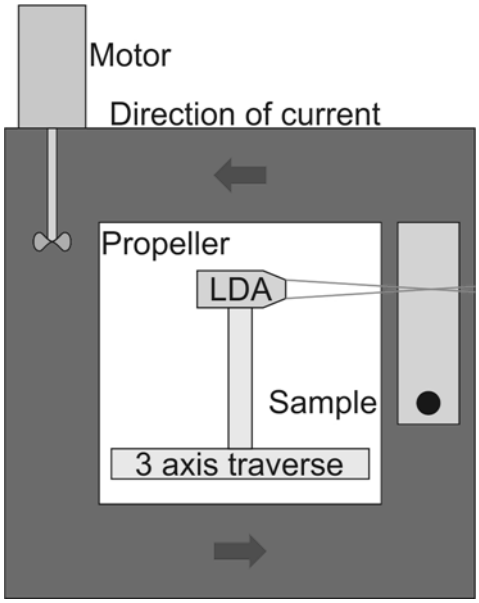

Figure 1. Schematic of experimental setup. The light grey region around the sample represents an acrylic window that allows the LDA laser light to enter the water flow.

3. Results and discussion

SEM images showing the size of the various sand fractions are shown in Figure 2a-d. The images show that the sand sizes are in the size range expected for each sieve size. Each sand fraction was glued to a glass slide in the same way that the hydrophobised

sand samples were made. The samples were then coated in gold so that they could be imaged using an SEM.

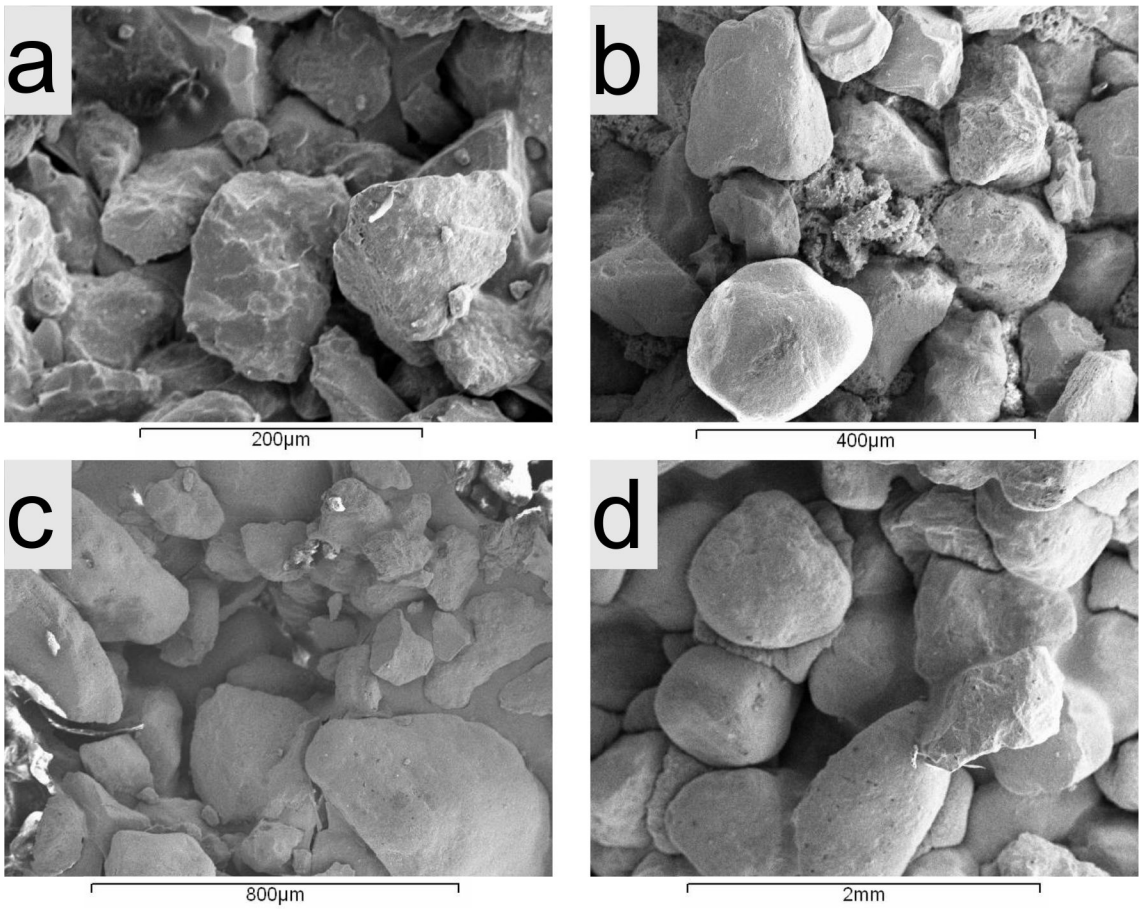

Figure 2. SEM images showing the sieved sand fractions. (a) 50-100µm, (b) 212-300µm, (c) 425-600µm and (d) 600-710µm.

The PDMS samples and sand-coated PDMS samples were characterised using static, advancing and receding contact angles. These were taken using a drop shape analysis system (Krüss DSA10). Advancing and receding contact angles were taken for all surface roughness values and for plain PDMS. The height of the sand from the substrate, the thickness of the plastron air layer after initial submersion and the thickness of the plastron after being subjected to a flow of water were all measured

using confocal microscopy. These confocal microscope measurements are needed because when the samples are placed in a flow of water some of the plastron air layer is stripped off of the surface. The measurements taken pre water flow show the plastron thickness as the sample is submerged in water and the plastron thickness taken post water flow show the thickness of the plastron as the drag reduction measurements are being taken. The samples were subjected to a flow of water for 10s to simulate the plastron stripping conditions experience in the flow chamber. The results from the drop shape analysis system and the confocal microscope measurements are shown in Table 1. A sample set of images from a confocal microscope stack are shown in Figure 3.

Sand size (μm)	Advancing contact angle (°)	Receding contact angle (°)	Roughness parameter (roughness scale/Cylinder diameter)	Sand thickness as measured by confocal microscopy (μm)	Plastron thickness pre water flow (μm)	Plastron thickness post water flow (μm)	Average sand protrusion height pre water flow (μm)	Average sand protrusion height post water flow (μm)
50-100	130±4	110±6	0.007± 0.004	133±46	125±47	82±27	8±61	52±49
212-300	131±5	112±8	0.018± 0.005	273±65	212±59	140±28	61±83	133±62
425-600	130±8	100±8	0.025± 0.006	364±56	301±49	176±29	64±70	188±56
600-710	130±5	95±2	0.06±0 .01	903±235	418±50	No plastron	485±190	903±235

TABLE 1. Contact angles, roughness parameters, sand thickness, plastron thickness and sand protrusion heights for various grain size samples before and after water flow treatment.

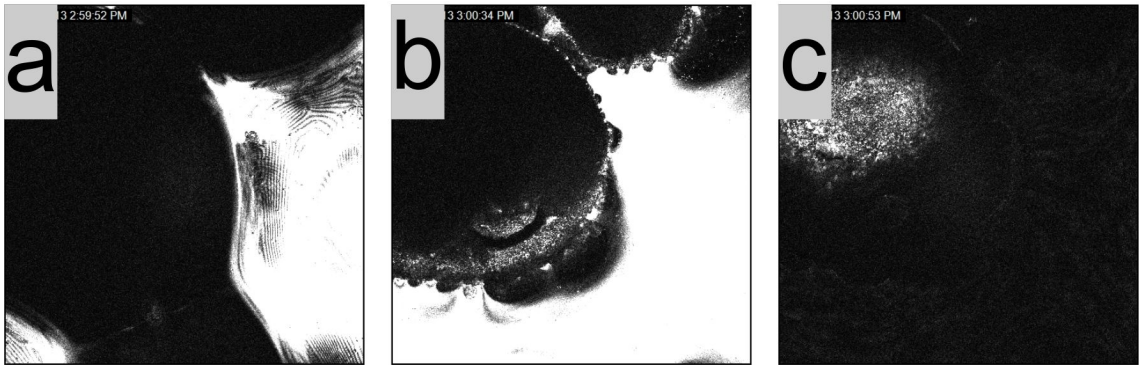

Figure 3. Images from a confocal microscope of 600-710μm sand pre water flow. (a) Shows the reflection from the PDMS surface. (b) Shows the reflection from the water-air interface at the plastron surface. (c) Shows the top of the sand protruding into the water.

To measure the drag coefficient of the PDMS rod and the hydrophobised sand coated rods they were placed into the flow chamber which was filled so that the rods were at a depth of 1.2m. Once the sample had reached this depth the motor was turned on and adjusted to allow the water to be circulated at speeds of $1.4ms^{-1}$ to $2.8ms^{-1}$. Measurements were taken using the momentum deficit technique[36]. Velocity profiles were taken 30 diameters downstream of the rod. The thickness of each sample was measured multiple times using callipers to find an average rod thickness. The LDA traversed from 60mm from the centre of the rod on one side to 60mm from the centre of the rod on the other side. This width of measurement was needed so that free stream velocities could be found. Results were obtained for the rods placed underwater

retaining a plastron layer and after being coated in ethanol which has the effect of preventing the formation of the plastron layer resulting in water coating all of the sand grains. This allows a direct comparison between the hydrophobic rods in the Cassie-Baxter state with the plastron air layer and the same rods in the Wenzel state without the air layer. The LDA results gave a velocity measurement at each point and when velocity was plotted against position a Gaussian profile was observed. A smooth Gaussian fit to the LDA data allowed the drag coefficient (C_D) value to be calculated using[36]

$$C_D = 2\int_{-\infty}^{\infty} \frac{U}{U_1}\left(\frac{U_1 - U}{U_1}\right) d\left(\frac{y}{d}\right),$$

where U_1 is the free stream velocity, U is the velocity at a given point as measured by the LDA, y is the horizontal displacement and d is the diameter of the rod being tested.

The results from the LDA measurements are shown in Figure 4. The average results from the plain PDMS coated rod, the rod with a plastron air layer and the rod with the ethanol pre-treatment are shown in each graph. Each graph shows experiments on each rod repeated a minimum of 5 times in its plastron bearing state and in its wetted out state.

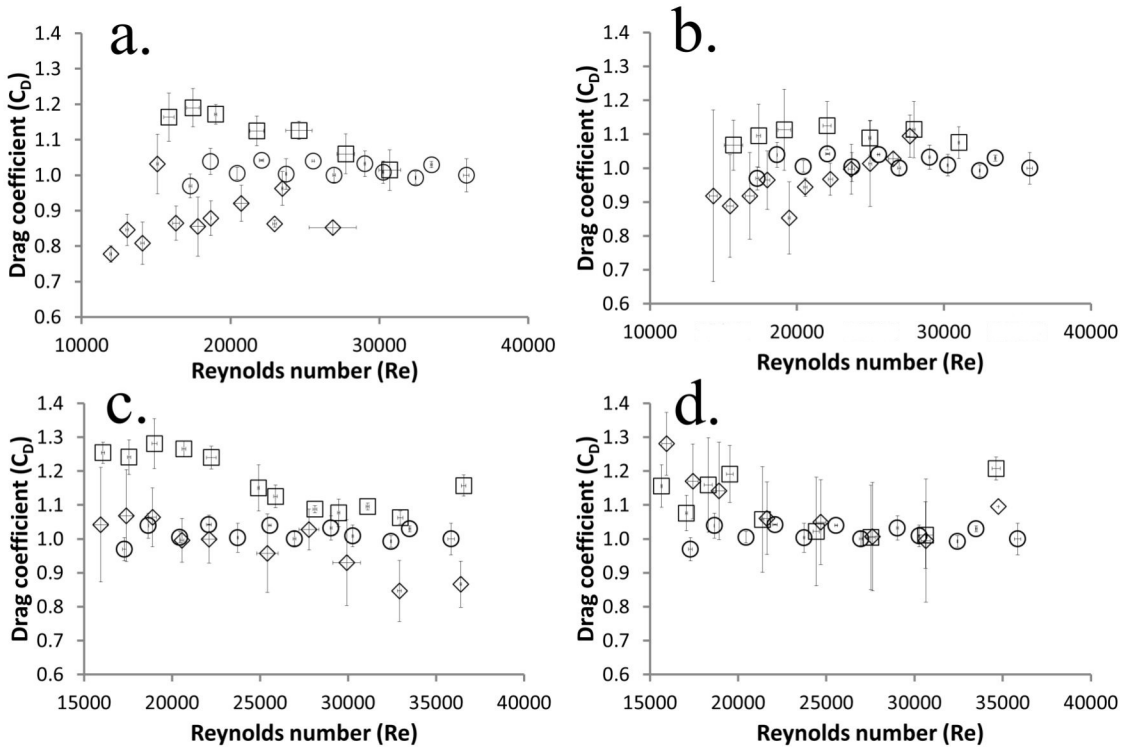

Figure 4. Variation of drag coefficient (C_D) at various Reynolds numbers (Re) for a 12mm diameter rod covered in various grain sizes of hydrophobised sand (diamonds), the same sand coated rod after a wetting out ethanol pre-treatment (squares) and a 12mm PDMS coated rod (circles). (a) 50-100µm sand, (b) 212-300µm sand, (c) 425-600µm sand and (d) 600-710µm sand.

The plain rod data in Figure 4 shows that in the Reynolds number range tested, the LDA results analysed with the momentum deficit technique gives results of ~1 which is what you would expect from book values[29]. The data for the ethanol pre-treated rods which do not have the plastron air layer, squares in the graphs in Figure 4, fits with the data for various roughness surfaces tested by Achenbach[28] although the roughness values shown in Figure 4b-c are of greater roughness parameter than shown by Achenbach.

The data shows that the largest drag reduction compared to the plain PDMS rod is seen with the 50-100µm hydrophobised sand. Both 212-300µm and 425-600µm sands show a drag reduction when compared to the plain PDMS rod at various Reynolds numbers tested. For the 212-300µm sand coated rod this drag reduction was seen at Reynolds numbers below 22,500. For the 425-600µm sand coated rod this drag reduction was seen at Reynolds numbers higher than 30,000. All samples show a reduction in the drag coefficient of the rod when comparing the sample to the same sample after it had the ethanol pre-treatment to remove the air layer except the 600-710µm rod which showed no signs of drag reduction across the Reynolds number range tested. This is expected due to the inability of the sample to retain a plastron even before the application of the ethanol pre-treatment. The advancing and receding contact angles of the sand sizes are shown in Table 1. All four sand sizes have similar results for advancing and receding angles. This shows that sands with similar contact angles can have significantly different plastron retention ability leading to large differences in drag reductions. These drag reduction results are consistent with the results from the confocal microscope experiments shown in Table 1. The results in Table 1 can be converted to a ratio of plastron thickness to protrusion height after the water flow was applied. This gives a ratio of 1.6 for the 50-100µm sand, 1.1 for the 212-300µm sand, 0.9 for the 425-600µm sand and 0 for the 600-710µm sand which was unable to retain a plastron. Figure 5 shows Drag reduction percentage vs the ratio of plastron thickness to protrusion height for all samples at Reynolds numbers of 17,500 and 25,000. The graph shows plots for the drag reduction achieved by a plastron bearing sample compared to the same sample wetted out.

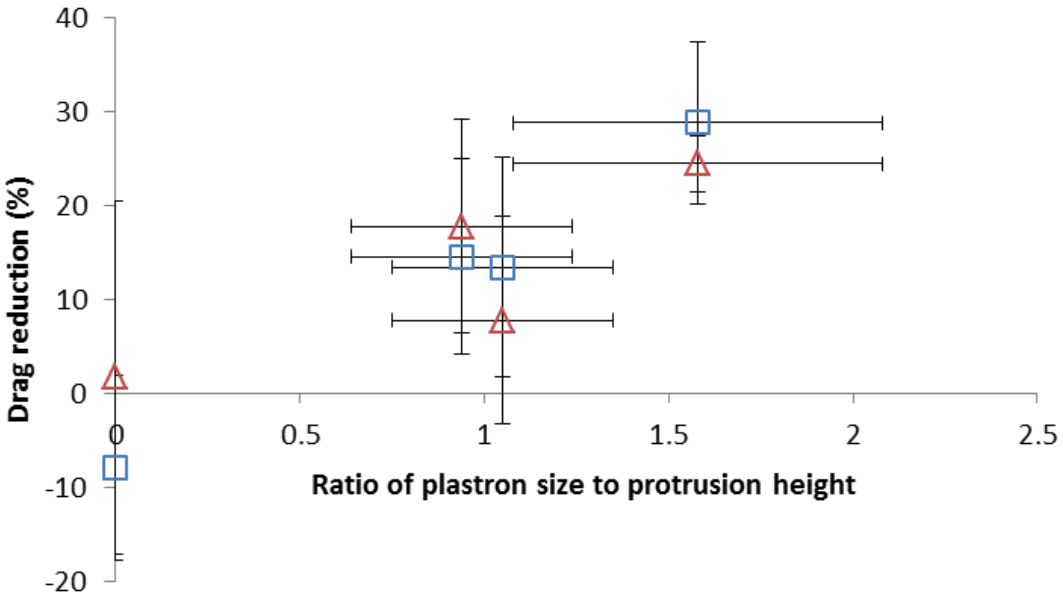

Figure 5. Drag reduction percentage versus ratio of plastron size to protrusion height for all sand sizes at 17500Re (triangles) and 25,000Re (squares) for plastron bearing samples compared to the same sample wetted out.

These ratios and drag reduction results shows that plastron thickness alone cannot be used to predict the magnitude of a drag reduction since both the 212-300µm and 425-600µm sands retained a thicker plastron layer than the 50-100µm sand. The drag reducing plastron thickness must be taken in conjunction with the drag increasing protrusion height of features for an effective drag reduction to be calculated.

4. Conclusions

In summary, hydrophobic rods and flat surfaces can be created by hydrophobising sand and using PDMS as a bonding layer to create substrates covered in the treated sand. The

surface roughness traps a plastron air layer which causes a drag reduction. A maximum drag reduction of 28% was achieved when comparing the plastron bearing samples to the same rod wetted out. The thickness of the plastron held by the roughness features and the protrusion height of the roughness features above the plastron both need to be taken in to account when predicting the drag reduction capabilities of a surface.

Acknowledgments

The authors wish to thank Professor Neil Sandham, Dr. Simon Stanley, Mr Brian Gruncell, Dr Steven Elliot and Mr Dave Parker for valuable discussions and help with experimental setup and Mr Gordon Arnott for help with microscopy. This work has been supported by the U.K. Engineering & Physical Sciences Research Council (EPSRC) under Grant EP/G057265/1. JCB is grateful to Nottingham Trent University for provision of Ph.D. studentship.

References

1. Roach P, Shirtcliffe N J and Newton M I 2008 *Soft Matter* **4** 224-240.
2. Barthlott W and Neinhuis C 1997 *Planta*. **202** 1-8.
3. Shirtcliffe N J, McHale G, Newton M I, Perry C and Pyatt F 2006 *Appl Phys Lett*. **89** 104106.
4. Flynn M R and Bush J W 2008 *J. Fluid Mech*. **608** 275-296.
5. Min T and Kim J 2004 *Phys. Fluids*. **16** 55-58.
6. Fukagata K, Kasagi N and Koumoutsakos P 2006 *Phys. Fluids*. **18** 051703.
7. Busse A and N. D. Sandham N D 2012 *Phys. Fluids*. **24** 055111.
8. B. R. K. Gruncell, Sandham and McHale G 2013 *Phys. Fluids*. **25** 0433601.

9. Busse A, Sandham N D, McHale G and Newton M I 2013 *J. Fluid Mech*. **727** 488-508.
10. Tsekov R and Boryan R 1999 *Intl. J. Miner. Process*. **56** 61-74.
11. Vinogradova O I 1995 *Langmuir*. **11** 2213-2220.
12. Rothstein J P 2010 Annu. *Rev. Fluid Mech*. **42** 89-109.
13. Vinogradova O I and Dubov A L 2012 *Mendeleev Communications* **22** 229-236.
14. Legendre D, Lauga E and Magnaudet J *J. Fluid Mech.* **633** 437-447.
15. Truesdell R, Mammoli A, Vorobieff P, Swoll F V and Brinker C J 2006 *Phys. Rev. Lett.* **97** 13012-13020.
16. McHale G, Shirtcliffe N J, Evans C R and Newton M I 2009 *Appl. Phys. Lett*. **94** 064104-064104.
17. Daniello R J, Waterhouse N E and Rothstein J P 2009 *Phys. Fluids*. **21** 085103.
18. Dong H, Cheng M, Zhang Y, Wei H and Shi F. *Journal of Materials Chemistry A*. **1** 5886-5891.
19. Srinivasan S, Choi W, Parks K, Chhatre S S, Cohen R E and McKimley G H 2013 *Soft Matter*. **9** 5691-5702.
20. McHale G, Flynn M R and Newton M I 2011 *Soft Matter*. **7** 10100-10107.
21. Muralidhar P, Ferrer N, Daniello R and Rothstein J P 2011 *J. Fluid Mech.* **680** 459-476.
22. Daniello R, Muralidhar P, Carron N, Greene M and Rothstein J P 2013 *J. Fluid Struct.* **42** 358-368.
23. McHale G, Newton M I and Shirtcliffe N J 2010 *Soft Matter*. **6** 714-719.
24. Choi C H and Kim C J 2006 *Phys. Rev. Lett*. **96** 066001.

25. Poetes R, Holtzmann K, Franze K and Steiner U 2010 *Phys. Rev. Lett*. **105** 166104.
26. Vakarelski I U, Patankar N A, Marston J O, Chan D Y and Thoroddsen S T 2012 *Nature*. **489** 274-277.
27. Vakarelski I U, Chan D Y, Marston J O and Thoroddsen S T 2013 *Langmuir*. **29** 11074-11081.
28. Lee C and Kim C J 2011 *Phys. Rev. Lett.* **106** 014502.
29. Catalano P, Wang M, Iaccarino G and Moin P 2003 *Int. Nt. J. Heat. Fluid. Fl.* **24** 463-469.
30. Fage A and Warsap J H 1929 Aero. Res. Com. Lordom, R. & M . no. 1283.
31. Achenbach E 1971 *J. Fluid Mech*. **46** 321-335.
32. Achenbach E and Heinecke E 1981 *J. Fluid Mech*. **109** 239-251.
33. Shih W C L, Wang C, Coles D and Roshko A 1993 *J. Wind Eng. Ind. Aerodyn*. **49** 351-368.
34. Verho T, Korhonen J T, Sainiemi L, Jokinen V, Bower C, Franze K, Franssila S, Andrew P, Ikkala O and Ras R H A 2012 *Proc. Natl. Acad. Sci*. (US). **109** 10210-10213.
35. Atherton S, Brennan J C, Morris R H, Smith J D E, Hamlett C A E, McHale G, Shirtcliffe N J and Newton M I 2014 *Materials* **7** 484-495.
36. Antonia R A and Rajagopalan S 1990 *AIAA Journal*. **28** 1833-1834.